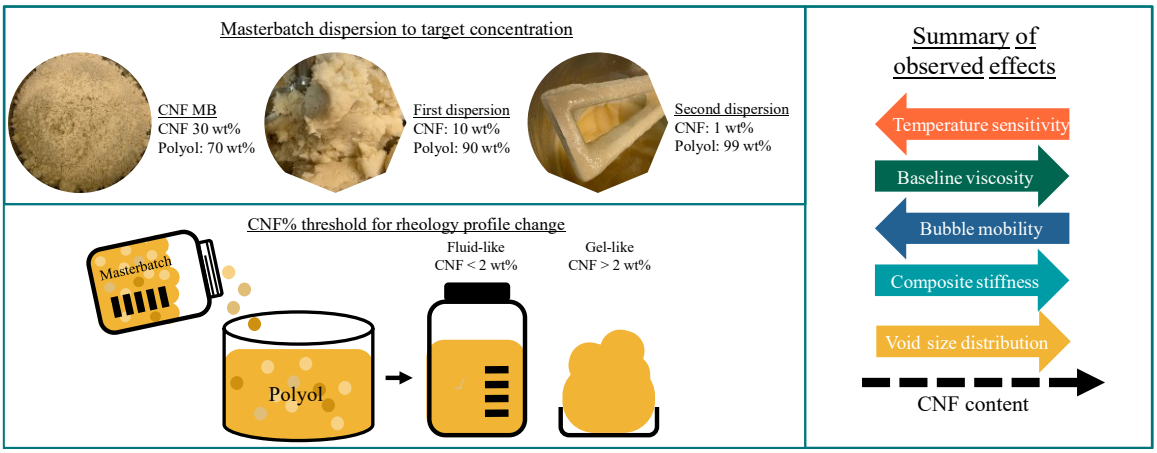
Rheological Behaviour of CNF-polyol Formulations and their Influence on Solvent-free PU Composites

Simen Prang Følkner [ab], Dag Molteberg [b], Jost Ruwoldt [c], Gary Chinga-Carrasco [c], and Kristin Syverud [ac]*

*Corresponding author: kristin.syverud@rise-pfi.no

DOI: 10.15376/biores.21.3.7949-7973

GRAPHICAL ABSTRACT



Rheological Behaviour of CNF-polyol Formulations and their Influence on Solvent-free PU Composites

Simen Prang Følkner [a,b] Dag Molteberg [b] Jost Ruwoldt [c] Gary Chinga-Carrasco [c] and Kristin Syverud [a,c*]

This study demonstrates an approach for incorporating cellulose nanofibrils (CNFs) into polyurethane (PU) using a solvent-free masterbatch consisting of 30% CNFs and 70% polyol, where the latter component functions as a carrier. This is the highest concentrated re-dispersible CNF-polyol system described to date. CNF addition produced strong shear-thinning behaviour, reduced the temperature sensitivity of viscosity, and maintained network integrity under conditions representative of PU curing. Power-law and Arrhenius modelling indicated that at low-to-medium shear rates the CNFs dominate rheological response, but the polyols rheological profile dominate at high shear rates when the fibrils occupy less space due to fluid flow alignment. Oscillatory tests showed increased elasticity and the transition from a viscous fluid toward gel-like behaviour at around 2% CNF loading. Cured CNF-PU composites exhibited increased stiffness, with microscopy revealing mechanically engaged fibrils within the fracture surfaces. Overall, CNFs provide an effective bio-based route to rheology modification PU systems, highlighting their potential in high-performance coatings and adhesives.

DOI: 10.15376/biores.21.3.7949-7973

Keywords: Nanocellulose; Fibrils; Thermoset composites; Coatings; Rheology; Reinforcement

*Contact information: a: Norwegian University of Science and Technology, Høgskoleringen 1b, NO-7034 Trondheim, Norway; b: Norske Skog Saugbrugs, Tistedalsgt. 9-11, NO-1772 Halden, Norway; c: RISE PFI, Høgskoleringen 6b, NO-7094 Trondheim, Norway; * Corresponding author: kristin.syverud@rise-pfi.no*

INTRODUCTION

Finding commercial avenues where nanocelluloses deliver value relative to incumbent solutions is key to motivating further industrial development. Nanocellulose shows high potential across rheology modification, suspension stabilization, and material reinforcement, but adoption is sometimes hindered by its high water content (Lee *et al*. 2014; Hubbe *et al*. 2017). High water content (i) adds significant packaging and shipping cost, (ii) can enable premature biodegradation during storage, and (iii) may interfere with moisture-sensitive formulation chemistries. The first concern can be mitigated by dewatering nanocellulose suspensions to ~10 to 20% solids (with some higher-solids grades available). The second concern can be mitigated by process handling and packaging choice. However, the third issue remains limiting. If waterborne nanocelluloses interfere in the chemistry of a product, it might render them as unsuitable or restricted to low dosages in water-sensitive formulations – often the systems where nanocelluloses can add the most value in large-volume industrial applications.

Thermoset systems are central to coatings, sealants, adhesives, and construction chemistry. They are usually classified as either waterborne, solventborne, high-solids or solvent-free, depending on their chemistry and content. All these thermoset classes rely heavily on rheology-modifying and reinforcing additives to function in the applications mentioned above – and the additives have varying degrees of compatibility with the overall systems depending on the classes and solvent choices. While solventborne thermoset systems and their accompanying additives are well explored and have been popular products for a while, these solutions are facing increasing regulatory pressures related to worker safety and environmental impact – for example, the EU restriction on intentionally added synthetic polymer microparticles (European Commission 2023), volatile organic compound (VOC) limits in decorative coatings (European Commission,2004), and broader initiatives under the EU Chemicals Strategy for Sustainability (European Commission 2025). This added scrutiny opens up potential opportunities for waterborne and solvent-free thermoset systems to capture new markets. This is a potential commercial avenue for nanocelluloses, as they are inherently non-VOC and biodegradable, allowing them to adhere to these regulatory constraints. While significant work has been conducted on the use of nanocelluloses in thermosets, particularly waterborne ones, their incorporation into solvent-free resin systems are often achieved through the use of drying techniques or solvent exchange – which may in fact re-introduce the restrictions mentioned above. Freeze-dried nanocellulose materials have a known limitation, namely hornification, consequently leading to poor re-dispersion, and this method also creates a powder that can be a potential inhalation hazard (Sinquefield *et al*. 2020; Wicklein *et al*. 2015; Yang *et al*. 2023). Solvent exchange requires the use and handling of volatile solvents, which adds to the process complexity and may significantly increase the carbon footprint of the dried nanocellulose. The authors' previous work has demonstrated that cellulose nanofibrils (CNFs) can be incorporated directly into solvent-free resins through the formation of highly concentrated masterbatches (MBs) (Følkner *et al*. 2026). This approach avoids the limitations associated with freeze-dried nanocellulose powders and solvent exchange routes. It is therefore interesting to explore CNF MBs usage in a variety of systems, especially those that can benefit both rheologically and mechanically from their implementation – such as polyurethane (PU) formulations.

Polyurethanes

Polyurethanes exist in both thermoplastic and thermoset forms, and distinguishing between them is critical (Hepburn 1992; Hinrichsen 1993; Magnin *et al*. 2020). PU materials consist of soft segments, derived from long-chain polyols, and hard segments, derived from reactions between diisocyanates and short-chain diols (chain extenders) that generate urethane linkages. The relative content and connectivity of these segments determine whether the material is flexible or rigid. Thermoplastic polyurethanes (TPUs) are produced primarily from di-functional polyols and diisocyanates, forming linear or lightly branched polymers. These materials may exhibit physical crosslinking through hydrogen bonding between hard segments, giving structural rigidity at low temperatures. Upon heating, these hydrogen-bonded associations weaken, and the material softens or melts, enabling reprocessing. While this confers recyclability, it also limits the mechanical and thermal stability of TPUs in high-temperature applications. By contrast, thermoset polyurethanes are formed when multifunctional polyols react with diisocyanates to form covalently crosslinked networks. These materials exhibit higher rigidity, dimensional stability, and chemical resistance, but they cannot be remelted or reprocessed. Working

with PUs or TPUs is nontrivial: Thermal degradation can produce volatile isocyanates, and at elevated temperatures hydrogen cyanide may form. In Europe, handling materials containing diisocyanates requires mandatory safety training under new REACH regulations, reflecting the hazards associated with these reactive species (European Commission, 2020).

Nanocelluloses and PUs – Challenge, Waterborne Polyurethanes (WPUs), Foams, Rheology

Significant research has been devoted to incorporating CNFs and cellulose nanocrystals (CNCs) into polyurethane systems to provide reinforcement or alter rheology. Nanocelluloses are generally produced and stored as aqueous suspensions, which poses a challenge for moisture-sensitive PU formulations. In conventional PU chemistry, polyols react with diisocyanates to form urethane linkages and crosslinked networks, but water can also react readily with isocyanates, generating CO_2 gas through a well-known blowing reaction (Randall and Lee 2002). This reaction is deliberately exploited in foam formulations; however, in castings and coatings the formation of bubbles is undesirable, because the resulting voids act as mechanical weak points (Saunders 1988) To prevent isocyanates from reacting with the water associated with nanocellulose, many researchers employ water-free approaches – either by using nanocellulose/polyol premixes *via* solvent exchange or by adding nanocellulose in dried powder form (Bello and Yan 2024; Leng *et al*. 2017; Zhou *et al*. 2016).

Waterborne polyurethanes (WPUs) provide another route for introducing nanocellulose into PU formulations (Noble 1997). WPUs consist of isocyanate-terminated prepolymers dispersed as submicron particles stabilized by ionic or nonionic surfactants. The reactive components remain segregated until the water evaporates, and the dispersed particles coalesce, allowing curing to proceed. As solventborne coatings face increasing regulatory scrutiny, WPUs have gained prominence, particularly in combination with nanocellulose.

A noteworthy observation by Pei *et al*. (2011) is that the hydroxyl groups on nanocellulose surfaces can react with isocyanates, potentially improving stress transfer from matrix to reinforcement. They observed rapid gelation when CNCs were added directly to 4,4′-methylenediphenyl diisocyanate (MDI), whereas no reaction occurred when CNCs were introduced into a stabilized WPU emulsion. Likely, the encapsulation of reactive groups inside dispersed prepolymer particles meant they were shielded from chemical interactions with the CNCs. The authors also suggest that CNCs can form covalent bonds with PU hard segments through hydroxyl-isocyanate reactions, whereas interactions with soft segments are weaker.

Nanocellulose-modified PU foams represent an active research area, and although not studied as part of this work, there have been reports suggestion that nanocelluloses can function as nucleation agents for PU foams – meaning that their addition introduces specific sites where gas bubbles begin to form. The idea is that nanocelluloses may help control pore sizes and pore shapes of the foam structure, which are significant factors in determining the foam materials ability to insulate against heat. Septevani *et al*. (2017) and Bello and Yan (2024) have both suggested that, respectively, CNCs and lignin-containing CNFs can act as nucleating agents – but there are some caveats to consider (Bello and Yan 2024; Septevani *et al*. 2017). The study by Septevani *et al*. (2017) showed an increase in closed cells when adding 0.4% CNC – leading to a reduction in thermal conductivity - but there were no significant changes in cell morphology, which would normally happen when

adding a nucleating agent – and this was not addressed by the authors. Bello and Yan (2024) did see a significant shift toward shorter average cell sizes for dosages of 0.1% CNF, but the effect of 0.2% CNF was less pronounced, which was suggested to be an issue with the higher loading causing a disruption of the foaming process. These studies across a narrow range of CNF/CNC addition neither address potential interactions between nanocelluloses and other additives (catalysts, co-catalysts and surfactants), nor the effects on the systems viscosity and stochiometric balance, or whether the hydroxyl groups on the cellulose surface potentially occupy water molecules that otherwise would function as a blowing agent. As such, current evidence is suggestive but not conclusive, and systematic studies are required to confirm a true nucleating effect.

In regards to the rheology of thermoset PU systems, the curing reaction is exothermic and the added heat initially produces a substantial drop in viscosity due to thermal thinning (Haseebuddin *et al*. 1996; Domínguez 2018). At this early stage, the material can become sufficiently fluid to sag on vertical surfaces, flow out of thick film applications, or migrate under pressure in adhesive joints. For this reason, PU formulations require rheology modifiers to stabilize the viscosity during the thermal maximum in the curing profile. However, many conventional rheology agents rely on hydrogen bonding or weak associative interactions, which are readily disrupted by heat. As a result, their viscosity-building effect diminishes as temperature rises, and formulators often must compensate by restricting the allowable coating thickness to avoid sagging on unevenness – instead applying coatings in multiple thin layers which avoid high-temperature curing schedules.

CNF-derived rheology differs fundamentally: Their network is stabilized predominantly through steric interactions, fibril entanglement, and mechanical percolation rather than hydrogen bonding alone (Iotti *et al*. 2011; Shafiei-Sabet *et al*. 2012). These interactions are far less sensitive to temperature increases, enabling CNFs to maintain its viscosity-building contribution even under the exothermic conditions typical of PU curing. This thermal robustness offers potential advantages in applications, where higher film builds, thicker adhesive lines, or elevated curing temperatures are desired.

Several studies report that nanocellulose induces shear-thinning behaviour in waterborne PUs, consistent with observations in aqueous nanocellulose systems. There are sometimes additional effects to be aware, such as Pei *et al*. (2011) finding that combining CNCs with MDI led to gelation, whereas CNCs added to stabilized dispersions did not, indicating that chemical interactions significantly affect rheology and processability. Similarly, Chen *et al*. (2021) showed that CNFs in combination with triethylamine (TEA) generated synergistic viscosity increases suitable for 3D-printing PU inks. While different classes of nanocelluloses will have varying surface chemistry, morphology, crystallinity and rheology profiles, these aforementioned examples underscore that nanocellulose-PU rheology depends not only on nanocellulose dosage but also on the process pathway and interactions with catalysts, surfactants, isocyanates, and formulation chemistry.

In this work, the rheological contributions of CNFs introduced into a solvent-free polyol *via* a masterbatch approach were investigated. It has previously been demonstrated in epoxy that adding CNF MBs to resin can introduce shear thinning properties and provide mechanical reinforcement, and this present study builds on this work by providing a more extensive rheological analysis and developing a model describing the influence of temperature and CNF concentration on viscosity (Følkner *et al*. 2026). Note that the polyol and curing agent used in this work are off-the-shelf products intended for solvent-free systems, that have not been modified to be compatible with CNFs – and these chemicals

are themselves not readily miscible in water. This is a conscious choice to highlight that the ability to transfer CNFs, typically processed in aqueous environments, into a non-aqueous system is therefore a distinguishing aspect of the present masterbatch approach.

EXPERIMENTAL

Materials

A masterbatch consisting of 30 wt% CNFs and 70 wt% polyol carrier was provided by Norske Skog Saugbrugs (Halden, Norway). This masterbatch is a commercial product, produced in industrial scale, based on RnD work by the first author. The CNFs had been mechanically processed and were produced from Northern Bleached Softwood Kraft (NBSK) pulp, and its morphology is described in previous work (Følkner *et al*. 2025). In that paper, the CNF-material used herein was fractionated and characterized in its aqueous state. More than 50% of the material passed through a 20 µm filter, and SEM analysis of this fraction revealed a fibril diameter ranging from 30 to 900 nm. While the exact fraction of fibrils below 100 nm was not quantified, a significant portion of the material fell within the nanoscale range. The material is therefore denoted as CNFs, in line with common usage, while acknowledging its polydispersity.

The commercial polyol used as both carrier and diluent was Merginol 240 (hydroxyl value 150 to 180 mg KOH/g; HOBUM Oleochemicals GmbH, Germany), which is based on soybean oil that has been modified with primary and secondary hydroxyl groups. The CNF MB was diluted with the same polyol to prepare samples containing 0.5, 1.0, 2.0, 5.0, and 10.0 wt% CNF. All CNF% values refer to oven-dry CNF mass fraction relative to total CNF + polyol. A reference of the neat polyol (designated CNF 0%) was also included. The soybean oil-based polyol used in this work is expected to have a relatively low overall polarity compared to aqueous systems typically used with nanocellulose. Simple qualitative mixing tests showed that the polyol does not readily mix with water, but instead forms a stable emulsion upon mechanical mixing. This indicates limited compatibility with water.

Polyurethane formulations were cured using a commercial diisocyanate (32.5% NCO; supplier not disclosed). The polyol and curing agent were mixed at a 1.0:0.5 weight ratio, corresponding to an isocyanate index of approximately 133 (±12).

Dispersion of CNF MB into Polyol

The CNF MB (30 wt% CNF) was first diluted to 10 wt% CNF by adding additional polyol. This intermediate dilution step ensured a high collision frequency between masterbatch granules, promoting efficient fibril dispersion. Mixing was performed using a proprietary butterfly mixer at 100 rpm for 6 h under vacuum (approx. –0.99 bar) at a set temperature of 35 °C. Due to friction at high CNF concentrations, temperatures occasionally increased to ~50 °C. These conditions ensured removal of entrapped air and evaporation of any moisture absorbed by the CNF or polyol.

The 10 wt% CNF mixture was subsequently diluted to the desired concentrations (0.5-5.0 wt% CNF) by adding more polyol and mixing for an additional 6 h under identical vacuum and temperature conditions.

Rheology

Rheometric measurements were conducted on an Anton Paar MCR 702e rheometer (Graz, Austria) equipped with 25 mm plate-plate geometry, which had a smooth surface. The measurement gap was set to 2 mm. The temperature was controlled using the P-PTD200/56 Peltier element and H-PTD200 hood. The sample was loaded onto the plate with a PLA spoon, followed by lowering the geometry to the measurement position and removal of excess fluid to match the manufacturer's specifications. After each measurement, the geometries were removed and cleaned with first water, followed by ethanol and at last acetone to remove all sample residues. Each data series was hence measured on a newly loaded fluid with no reuse of old samples.

Shear Rate Sweep

The sample was heated to the desired temperature, followed by pre-shearing at 100 s^{-1} for 120 s. Afterwards, the measurement commenced in continuous shear mode going from 0.01 s^{-1} to 1000 s^{-1} with a logarithmic increase in shear rate. Ten points per decade were measured with 10 s measurement duration for each data point.

Strain Sweep

The sample was heated to the desired temperature, followed by pre-shearing at 100 s^{-1} for 120 s and quiescent rest for 60 s. Afterwards, the oscillatory measurement started by logarithmically increasing from 0.001% to 10% strain at 1 Hz. Ten data points were measured per decade, where each point had a measurement duration of 10 s. The region below 0.01% was omitted from further analysis and discussion due to poor reproducibility. The elastic shear stress τ_{el} was calculated from the measured storage modulus G' and strain γ using Hooke's Law for shear as in Eq. 1.

$$\tau_{el} = \gamma G' \quad (1)$$

Frequency Sweep

The sample was heated to the target temperature, followed by pre-shearing at 100 s^{-1} for 120 s and subsequent quiescent resting for 60 s. Following this, the oscillatory measurement was initiated, which went from 0.01 to 100 Hz at a strain of 0.04%. This increase was again done logarithmically with 10 data points per decade and 20 s measurement time per point. The region below 0.1 Hz was omitted from further analysis and discussion due to poor reproducibility.

Composite Curing

Polyol samples containing 1.0% and 2.0% CNF were cured with the diisocyanate curing agent at a 1.0:0.5 polyol-to-isocyanate weight ratio, yielding final CNF contents of 0.67% and 1.33%, respectively. The neat polyol was cured under identical conditions. The chemicals were mixed using a glass stirring rod, at a slow pace to reduce incorporation of air. After mixing, the samples were placed in a vacuum chamber for 15 minutes to remove bubbles. Then, the samples were left for 24 hours to cure in room temperature (22 °C), before post-curing at 55 °C in an oven for 12 hours. Initial curing trials revealed bubble formation in the neat polyol, indicating residual moisture; therefore, the polyol was dried at 105 °C for 24 h prior to composite preparation.

Specimen Preparation of Cured Samples

Specimens were cut from the cured composite boards using a Twotrees TTC450 PRO CNC Router (gSender 1.4.11, Sienci Labs, Waterloo, Canada). CAD models were prepared in SolidWorks. Dog-bone specimens for tensile testing (10 × 65 × 3.5 mm), and rods for Charpy impact specimens (10 × 75 × 10 mm with a 2 mm notch) were machined from the boards. Rectangular blocks were used for pendulum impact testing. Due to restricted access to the curing agent, limited numbers of specimens were produced per sample: Two to three specimens for impact testing and three to four specimens for tensile testing.

Mechanical Testing

Tensile testing of the dog-bone specimens (three per formulation) was performed using a Zwick Roell Zmart.Pro (Ulm, Germany) equipped with a 2.5 kN load cell and a clip-on extensometer. Tests were conducted at a crosshead speed of 2 mm/min. Pendulum impact testing was carried out using a Zwick Roell HIT5.5P (Ulm, Germany).

Microscopy

Scanning electron microscopy (SEM) images were acquired with a Hitachi SU3500 scanning electron microscope, in backscatter mode (BSE), coated with carbon.

RESULTS AND DISCUSSION

Rheology Measurements

Measurements were conducted on neat polyol and the CNF-polyol mixtures – prior to the curing agent being added. During method development, it became clear that the CNF-containing samples exhibited only limited thixotropy but showed pronounced instability under certain shear conditions. Continuous shear measurements revealed that samples with higher CNF loadings became unstable at shear rates slightly above 10 s^{-1}. At these shear rates, the material began to roll up into localized aggregates within the plate-plate gap, which could subsequently be squeezed out from between the plates. This resulted in abrupt drops in apparent viscosity and, in extreme cases, loss of contact between the sample and the geometry.

Notably, this behaviour was not observed when the samples were pre-sheared at 100 s^{-1}. A sufficiently high pre-shear rate appeared necessary to fluidize the fibrillar network and disrupt weak, sample-spanning structures that otherwise caused aggregation under moderate shear. Pre-shearing also eliminated inconsistencies originating from sample loading, providing a controlled and reproducible shear history prior to measurement. The selected pre-shear conditions were chosen empirically: higher shear rates caused immediate sample ejection during pre-shear, whereas lower rates were insufficient to eliminate the aggregation phenomenon or led to similar instabilities during the subsequent measurement.

The gap height of 2 mm also represents the optimum condition determined by trial-and-error; smaller gaps would aggravate sample aggregation and ejection, whereas larger gaps provided insufficient contact between the sample and the plate-plate geometry. These effects also contributed to the choice of plate-plate over cone-plate geometry, where the narrow gap caused premature material expulsion and hence prevented stable measurements. Although plate-plate geometries introduce a non-uniform shear field –

lower shear rates near the centre and higher toward the rim – the rheometer reports an effective shear rate averaged over this distribution. For non-Newtonian materials such as CNF/polyol mixtures, this averaging can introduce deviations, including those observed when fitting the data to the Ostwald-de Waele (power-law) model. Nonetheless, the overall trends and relative comparisons remained valid, and the methodology provided reproducible data across the range of CNF concentrations investigated.

No clear evidence of significant CNF agglomeration was observed in the prepared systems. The rheological behaviour was consistent and reproducible, without indications of anomalies that would suggest large agglomerates. SEM observations likewise did not reveal obvious clustered regions, although such methods may not capture all forms of nanoscale aggregation.

Shear Rate Sweep

Figures 1 and 2 show the apparent viscosity of the samples at 20 °C and 50 °C over a wide range of shear rates, the latter temperature representing conditions typical of an exothermic polyurethane curing process. At 50 °C, the reference sample containing no CNF (0% CNF; neat polyol) displayed essentially Newtonian behaviour, whereas at 20 °C the same material exhibited mild shear-thinning. This indicates that increased temperature can enhance segmental mobility within the polyol, leading not only to a substantial reduction in viscosity but also to a suppression of non-Newtonian effects. The magnitude of the thermal thinning is significant: At a shear rate of 1 s^{-1}, increasing the temperature from 20 to 50 °C reduced the viscosity of the neat polyol from 4927 to 492 mPa·s – a decrease of approximately 90%. Such a pronounced viscosity drop illustrates why PU coatings and adhesives typically require rheology modifiers to prevent sagging, dripping, or flow during the early stages of cure. The temperature dependence of the neat polyol followed an Arrhenius-type relationship, as will be discussed in later.

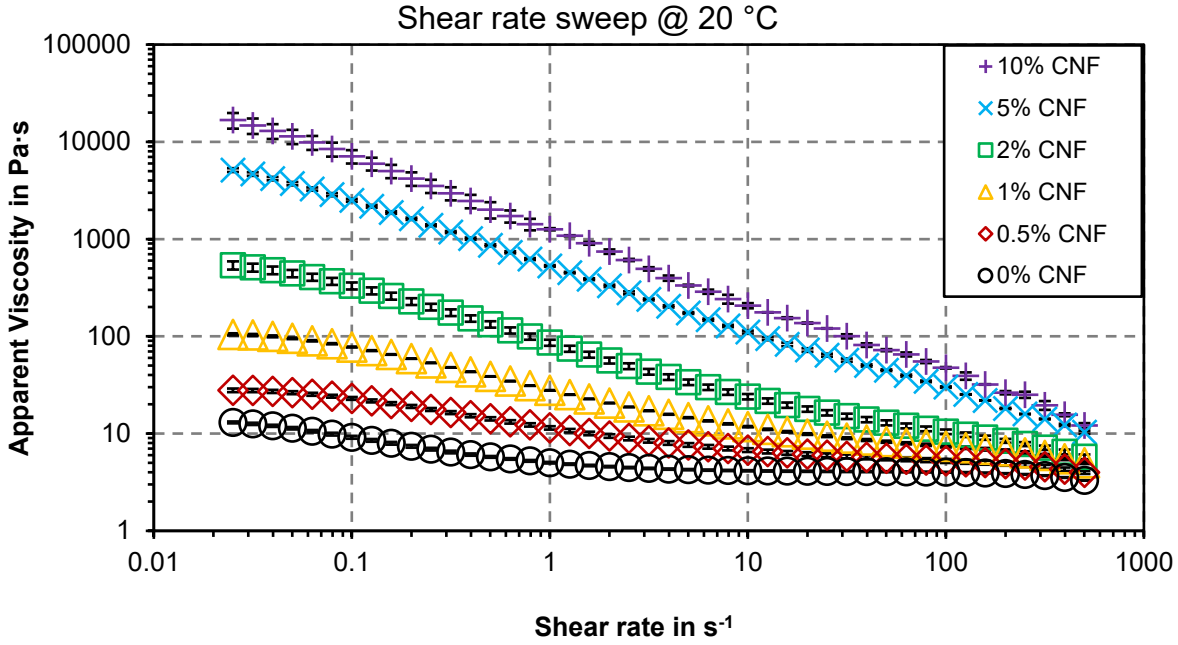


Fig. 1. Shear rate sweep of samples with increasing CNF content in polyol at 20 °C

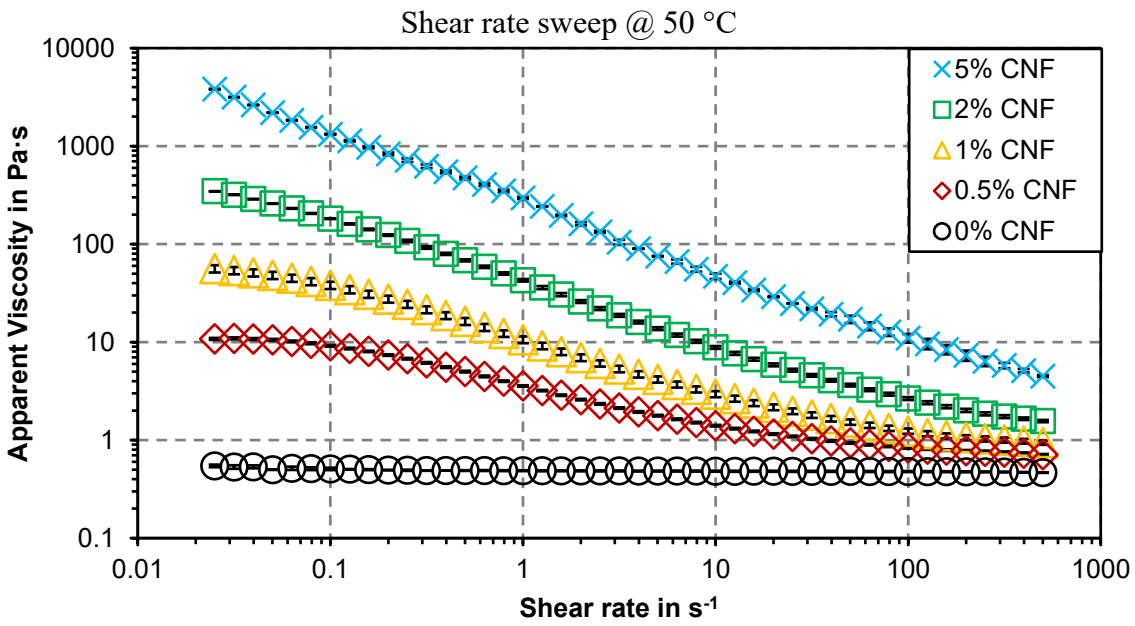


Fig. 2. Shear rate sweep of samples with increasing CNF content in polyol at 50 °C

All CNF-containing formulations displayed clear non-Newtonian behaviour, characterized by pronounced shear thinning across the entire shear-rate range. This is consistent with the expected behaviour of fibrillar suspensions, where an extended entangled network contributes to high low-shear viscosity and progressive alignment of fibrils under shear reduces resistance to flow. As anticipated, increasing the CNF concentration increased the measured apparent viscosity at all shear rates.

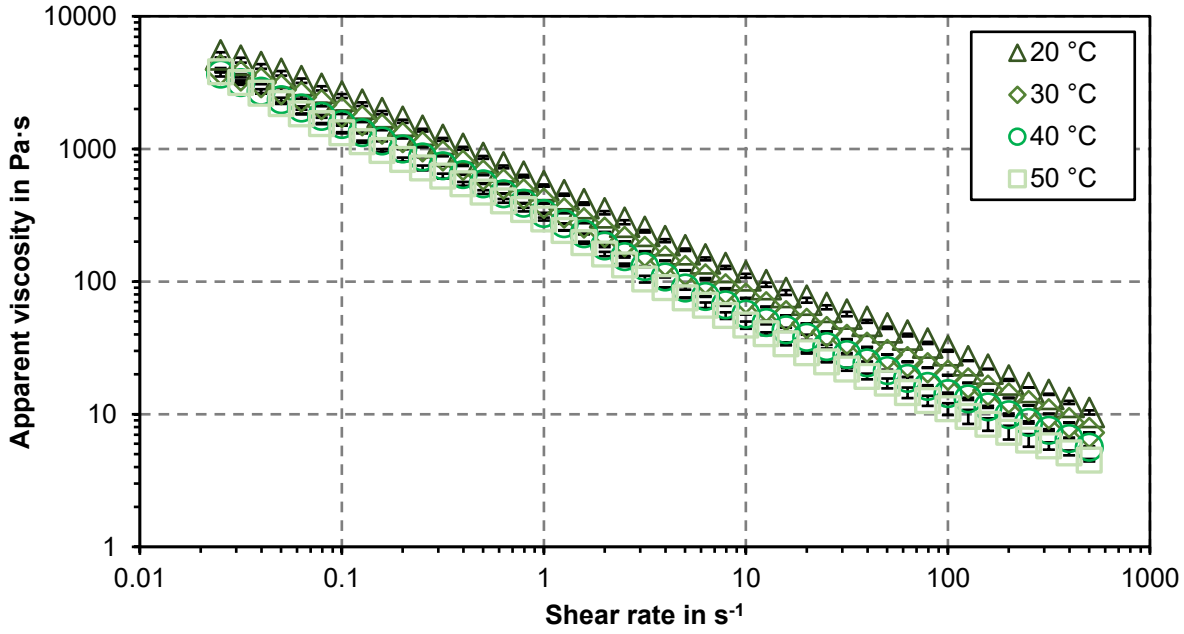


Fig. 3. Effect of temperature on the apparent viscosity during shear rate sweeps of the sample with 5% CNF in polyol

Figure 3 illustrates the temperature dependence of the 5% CNF sample across several temperatures. Although viscosity decreased with increasing temperature, the reduction was less pronounced than that observed for the neat polyol, *i.e.*, without CNF addition. Importantly, the characteristic shear-thinning profile remained intact across the temperature range, demonstrating that the CNF network retains its structural integrity under the thermal conditions representative of PU curing. The temperature effects are explored further in the modelling section.

Rheology Modelling

The shear-rate-dependent behaviour of the samples was modelled using the power-law fluid model (Ostwald-de Waele relationship) (Barnes *et al*. 1989; Bird *et al*. 2006), which relates shear stress τ to shear rate $\dot{\gamma}$ through Eq. 2.

$$\tau = K(T)\dot{\gamma}^n \tag{2}$$

Here, $K(T)$ is the flow consistency index (reflecting viscosity at a reference shear rate), and n is the flow behaviour index ($n < 1$ indicating shear-thinning behaviour).

Overall, the power-law model captured the qualitative shear-thinning behaviour of all formulations, as shown in Fig. 4. For the neat polyol (0% CNF), the model fit improved substantially at 50 °C, consistent with the fluid exhibiting Newtonian behaviour at elevated temperature ($n \approx 1$). In contrast, the fit quality for CNF-containing samples decreased at 50 °C, particularly for the 1% and 2% CNF formulations, which showed the greatest deviations at both temperatures. A systematic pattern was observed: the fitted curves tended to (i) underestimate shear stress at low shear rates (~0.01-1 s^{-1}), (ii) overestimate in the mid-range (~1-100 s^{-1}), and (iii) again underestimate at the highest shear rates (>100 s^{-1}). Such deviations could be expected when applying a simple two-parameter model to complex fibrillar suspensions exhibiting different structural regimes under varying shear. Moreover, the inhomogeneous shear rate profile imposed onto this non-Newtonian fluid by the plate-plate geometry could be a cause. Albeit not providing a perfect fit, the data were still in good agreement with the model at an R^2-value of > 95% for all samples.

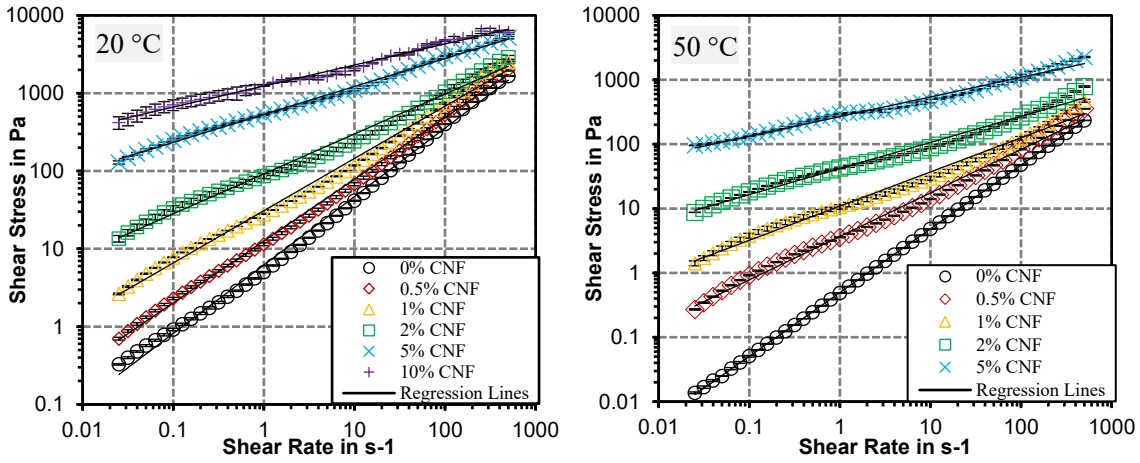


Fig. 4. Shear stress vs shear rate plots and regression lines using the Ostwald-de Waele relationship for various CNF loadings in the polyol at two different temperatures

From the fitted parameters in Table 1, all samples had flow behaviour indices n below 1, confirming pseudoplastic behaviour. Increasing temperature shifted n toward

unity for the neat polyol; at 50 °C, the value $n \approx 0.99$ virtually implies Newtonian behaviour. Increasing CNF concentration decreased n, indicating stronger shear-thinning behaviour associated with more extensive fibrillar networks.

The flow consistency index K in Table 1 decreased when temperature was increased from 20 to 50 °C, for all samples, reflecting lower viscosity at elevated temperatures. However, the magnitude of this decrease varied significantly. The neat polyol exhibited a ~92% reduction in K from 20 to 50 °C, whereas CNF-containing samples showed much smaller reductions (50 to 71%), depending on CNF loading. Thus, CNF not only increased baseline viscosity but also substantially reduced temperature sensitivity, preserving elevated viscosity under thermal conditions representative of PU curing.

Table 1. Ostwald-de Waele relationships of CNF/polyol samples

CNF content	Temperature	Flow consistency index *K*	Flow behaviour index *n*	Line fit R^2
%	*°C*	*Pa·s^n*	-	-
0.0%	20	6.2	0.8799	0.9988
0.5%	20	12.6	0.7938	0.9984
1.0%	20	30.9	0.6719	0.9946
2.0%	20	91.8	0.5132	0.9870
5.0%	20	533.9	0.3590	0.9971
10.0%	20	1236.0	0.2707	0.9868
0.0%	50	0.5	0.9902	0.9999
0.5%	50	3.7	0.6754	0.9821
1.0%	50	10.9	0.5307	0.9589
2.0%	50	41.8	0.4059	0.9553
5.0%	50	268.2	0.3049	0.9761

Arrhenius-Type Temperature Dependence

The temperature dependence of viscosity was further analysed using an Arrhenius-type relationship, which is widely used to describe viscosity-temperature behaviour in polymeric and crosslinking systems (Montarnal *et al*. 2011; Williams *et al*. 1955). The Arrhenius expression for viscosity is given in Eq. (3),

$$\eta = Ae^{\frac{E_A}{RT}} \tag{3}$$

where A is the pre-exponential factor, E_A is the activation energy for viscous flow, R is the gas constant, and T is the absolute temperature. Higher activation energy E_A indicates stronger temperature sensitivity, as the term is divided by the temperature in the exponent. The Arrhenius equation is frequently used in the linearized form, (see Eq. (4)), which allows determination of the pre-exponential factor A as the y-intercept and the activation energy E_A from the slope.

$$\ln \eta = \ln A + \frac{E_A}{R}\frac{1}{T} \tag{4}$$

Arrhenius plots for the 5% CNF formulation are shown in Fig. 5 (left), with linear fits and fitting equation parameters. Figure 5 (right) compares model predictions with

experimental viscosities. The Arrhenius model provided a satisfactory fit, with predicted values falling largely within the experimental error.

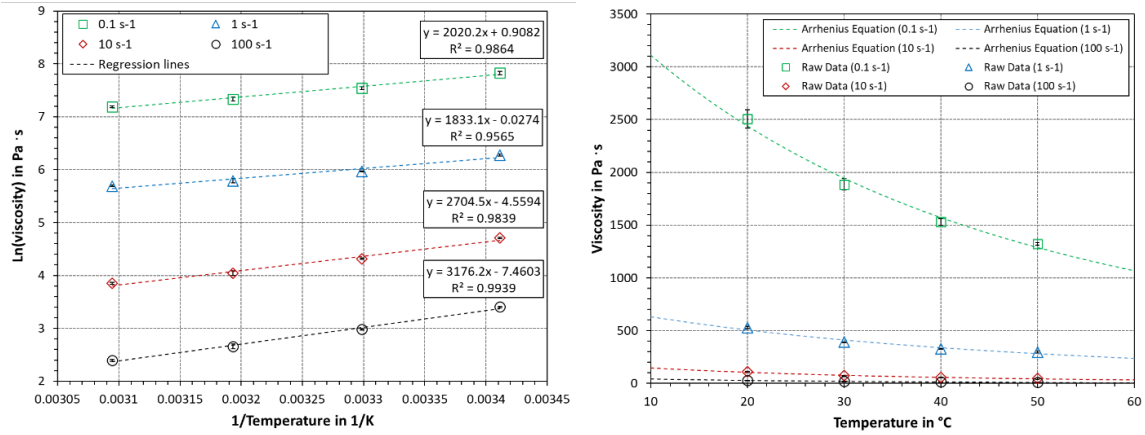


Fig. 5. Arrhenius plots of 5% CNF; straight line equation (left), model lines w/ experimental data (right)

This modelling furthermore made it possible to determine the pre-exponential factor A and the activation energy E_A. The values are listed below in Table 2.

Table 2. Fitting Parameters from the Arrhenius Equation Model

CNF content	Shear Rate	Pre-exponential factor *A*	Activation Energy *Ea*
%	*s^{-1}*	*Pa·s*	*kJ/mol*
0.0%	0.1	$2.7 \cdot 10^{-13}$	75.9
0.0%	1	$6.1 \cdot 10^{-11}$	61.3
0.0%	10	$3.5 \cdot 10^{-10}$	56.5
0.0%	100	$4.5 \cdot 10^{-10}$	55.8
0.5%	0.1	$1.2 \cdot 10^{-3}$	24.1
0.5%	1	$4.1 \cdot 10^{-5}$	30.6
0.5%	10	$2.9 \cdot 10^{-7}$	41.3
0.5%	100	$1.3 \cdot 10^{-8}$	48.2
1.0%	0.1	$3.5 \cdot 10^{-2}$	18.7
1.0%	1	$8.3 \cdot 10^{-4}$	25.4
1.0%	10	$3.9 \cdot 10^{-6}$	36.4
1.0%	100	$3.1 \cdot 10^{-8}$	47.0
2.0%	0.1	$5.2 \cdot 10^{-1}$	15.7
2.0%	1	$4.5 \cdot 10^{-2}$	18.4
2.0%	10	$5.0 \cdot 10^{-4}$	26.2
2.0%	100	$4.1 \cdot 10^{-6}$	35.9
5.0%	0.1	2.5	16.8
5.0%	1	$9.7 \cdot 10^{-1}$	15.2
5.0%	10	$1.0 \cdot 10^{-2}$	22.5
5.0%	100	$5.8 \cdot 10^{-4}$	26.4

For the 5% CNF formulation, four temperatures enabled a robust regression; for the other loadings, two-point fits were mathematically exact but did not permit goodness-of-fit evaluation. These parameters should therefore be interpreted cautiously, although it is reasonable to assume similar Arrhenius-type behaviour for all compositions. Despite these limitations, several trends clearly emerged. Increasing CNF content led to progressively lower activation energies E_A, indicating reduced temperature sensitivity in CNF-rich systems compared with the neat polyol. Meanwhile, the pre-exponential factor A increased with CNF loading, consistent with higher baseline viscosity due to fibrillar network formation.

Interestingly, for all CNF-containing samples, E_A increased and A decreased under conditions involving more intense shear. This suggests that fibril network structure and orientation significantly influence thermal-rheological behaviour. Higher shear promotes fibril alignment and closer packing, reducing fibril-fibril interactions and lowering base viscosity. In this more aligned state, the polyol matrix occupies a greater proportion of the load-bearing flow field, increasing its influence on temperature-dependent viscosity. This shift likely contributes to the observed rise in E_A, as the system's thermal sensitivity begins to resemble that of the polyol itself.

Strain Sweep

The strain sweep characterizes how much deformation a material can withstand before its internal structure is irreversibly changed. This measurement identifies (i) the linear viscoelastic (LVE) region, in which the storage modulus (G') and loss modulus (G'') remain constant with increasing strain and the material deforms reversibly, and (ii) the yield point, defined here as the shear stress recorded at the end of the LVE regime. Between these two regimes lies a softening zone in which the internal structure begins to reorganize. As discussed previously, CNF-based rheology is relatively insensitive to temperature due to its steric and entanglement-based network structure, suggesting that CNF-containing formulations can maintain their LVE region during the exothermic curing of thermoset coatings – an advantage over rheology agents whose function degrades at elevated temperatures.

As shown in Fig. 6, the LVE region extended to approximately 0.1% strain for both the 2% and 10% CNF formulations. Below this threshold, both G' and G'' remained constant, confirming LVE behaviour. Although the magnitude of G' increased substantially with CNF content – reflecting a stiffer fibrillar network – the extent of the LVE region did not increase. Thus, increasing CNF loading increased the materials elastic response, but did not enhance the extent of the LVE region. Based on these observations, a strain amplitude of 0.04% was selected for subsequent frequency sweeps to ensure operation well within the LVE regime.

To determine the yield point, the storage and loss moduli were also plotted with respect to shear force in Fig. 6. Here, the yield point was identified as the shear force, at which the storage modulus G' started to significantly decrease. This decrease was determined according to Rouyer *et al*. (2005) using straight lines fitted to the start and end points of the data in the log-log plot. For the 2% CNF sample, the yield point occurred at approximately 3.0 Pa shear force. In contrast, for the 10% CNF sample, the yield point was elevated to 160.6 Pa. This indicates that the highest CNF loading required greater stresses to fully disrupt the network and achieve flow. Such behaviour is consistent with a more strongly connected fibrillar network that resists complete breakdown under the applied oscillatory deformation.

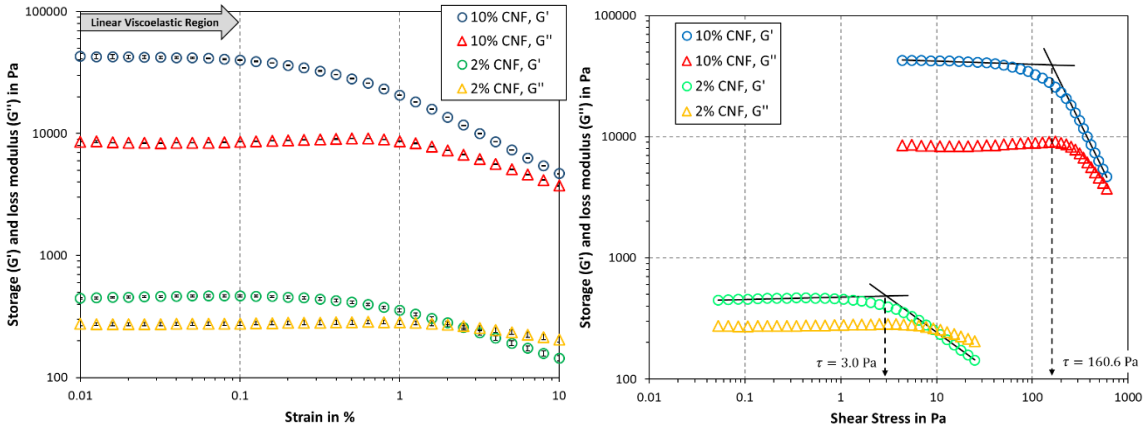


Fig. 6. Strain sweep at 20 °C and 1 Hz for two distinct CEBINA loadings

For CNF dispersions, these transitions from LVE region to the softening phase, to the yield point, can be interpreted in terms of the fibrillar network's structure. Within the LVE region, the deformation is sufficiently small that the percolated network remains intact and responds elastically. As strain increases beyond the LVE limit, reversible microstructural damage occurs: Entanglements and contact points slip or partially disengage, leading to a decrease in G'. At the yield point, connectivity within the network is sufficiently reduced that elastic behaviour can no longer dominate, and the system transitions to viscous flow. Beyond yield, fibrils move relative to one another with reduced resistance and the material behaves more like a viscous dispersion.

Frequency Sweep

The frequency sweep probes the viscoelastic behaviour by varying the oscillation frequency while maintaining a strain amplitude within the LVE region. This test reveals whether the material behaves more like a viscoelastic fluid or a gel. A material is said to be at the gel point, if its steady shear viscosity is infinite and its equilibrium modulus is zero (Winter and Chambon, 1986). In practical terms, a viscoelastic fluid tends to exhibit a greater loss (G'') than storage modulus (G') at low frequencies, whereas a gel shows greater storage modulus over a wide range of frequencies. These circumstances can also be formulated in terms of the phase angle, which is closer to 90° for viscoelastic fluids and closer to 0° for gels. Viscoelastic fluids typically show an intersection of the storage modulus (G') and loss modulus (G'') within the measured frequency range, whereas gel-like materials exhibit nearly parallel G' and G'' curves that do not intersect (Simon *et al*. 2015). The frequency sweeps of the various CNF suspensions and the reference are shown in Fig. 7.

The 0.5% and 1% CNF formulations showed behaviour characteristic of viscoelastic fluids: G' and G'' approached one another and intersected within the accessible frequencies. In contrast, the 5% and 10% CNF samples displayed distinctly gel-like signatures. Their G' and G'' curves progressed in roughly parallel fashion below ~1 Hz, and no intersection between the moduli was observed. The 2% CNF formulation exhibited intermediate characteristics, consistent with a partially percolated but not fully gelled fibrillar network. At frequencies above ~5 Hz, a marked increase in G'' was observed for all samples with ≤ 2% CNF. For the 2% CNF sample, the storage and loss moduli were closest in magnitude around 8 Hz, although convergence without intersection suggests that elastic contributions still dominated the response at this strain amplitude.

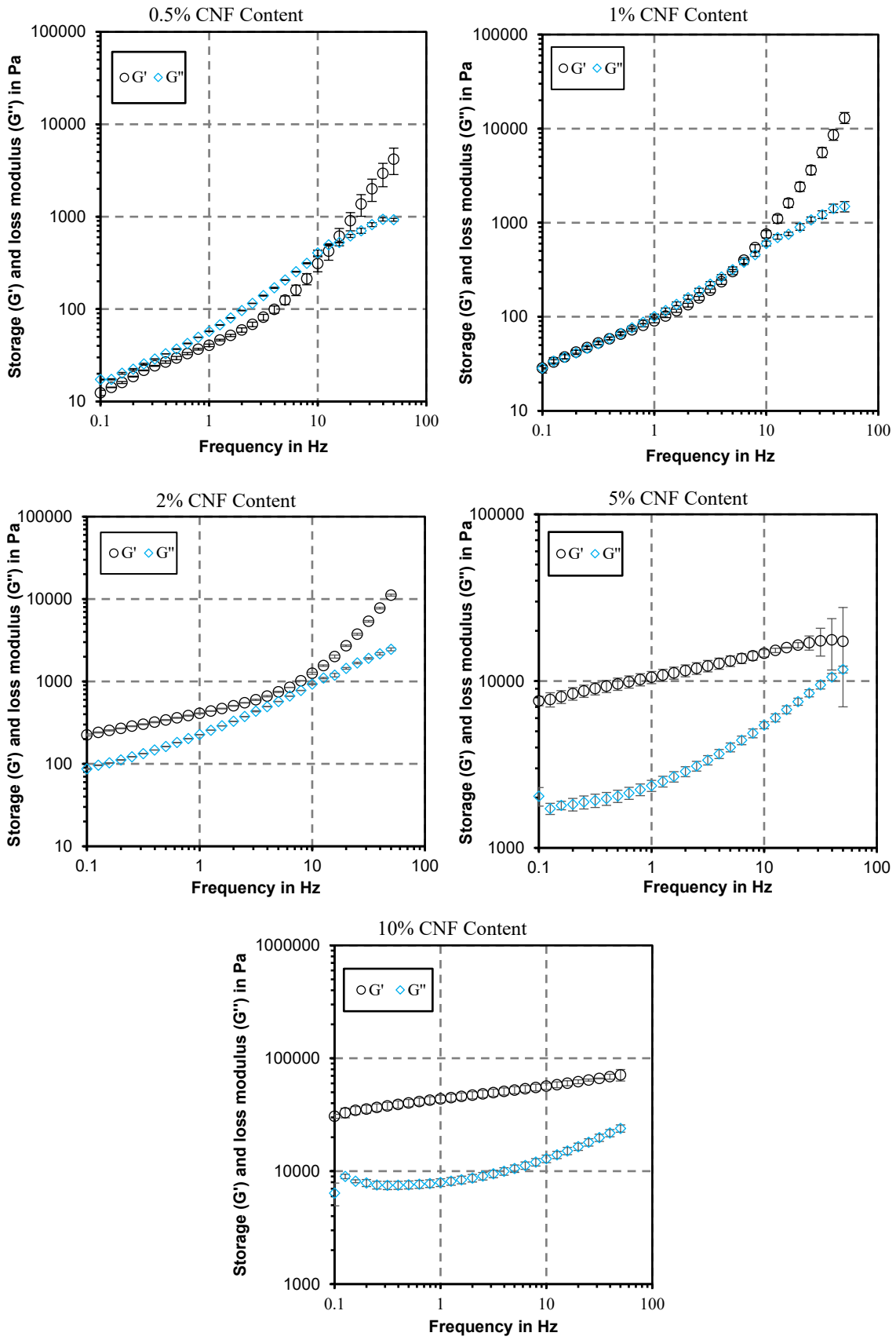


Fig. 7. Frequency sweep for various CNF loadings in the polyol at 20 °C

Data above 50 Hz were excluded due to poor reproducibility. At high oscillation frequencies, the corresponding shear rates become large, increasing the likelihood of amplitude overshoot, sample edge fracture, and other measurement instabilities. These artefacts introduce significant error, making data in this region unreliable for interpretation.

To provide a better overview, the phase angles of the measurements in Fig. 7 were also plotted and compared in Fig. 8. As can be seen, the phase angle was between 40 and 60° for 0.5% and 1% CNF below 10 Hz. For 5% and 10% CNF, the phase angle was below 20° within the same frequency range. The sample with 2% CNF showed the same qualitative progression of phase angle as the samples with 0.5% and 1% CNF, however, quantitatively the data series was located in between the graphs for the phase angles of higher and lower CNF content. This highlights the previously outlined trend: A CNF content of ≤ 1% exhibiting the behaviour closer to that of a viscoelastic fluid, whereas ≥ 5% CNF was closer to a gel and 2% CNF lay within a transition region.

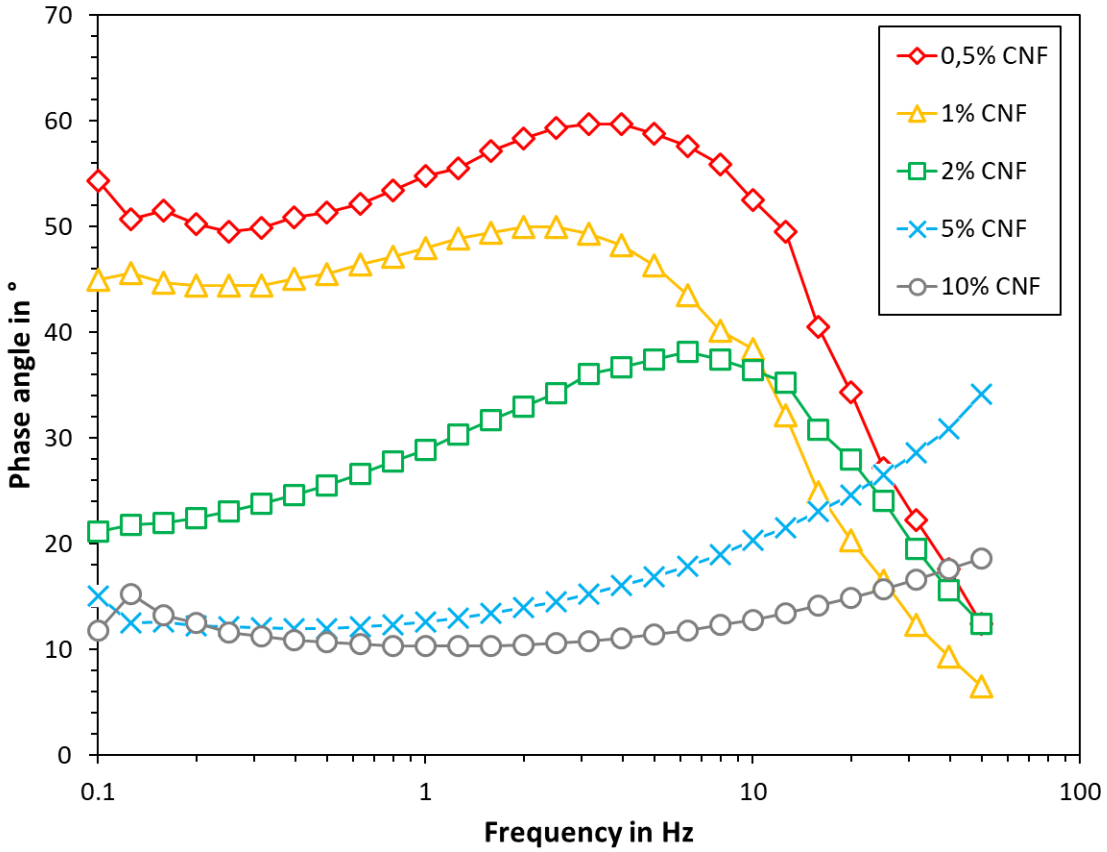


Fig. 8. Phase angles of the frequency sweep for various CNF loadings in the polyol at 20 °C

Cured Samples: Preparations and Observations

Polyol samples that had been used in prior rheology studies containing 0%, 1% and 2% CNF were cured with diisocyanate, yielding composites with final CNF contents of 0.0 %, 0.67% and 1.33%, respectively. There was limited access to diisocyanate. As such, only three systems were cured for testing – with the ones chosen being most relevant dosages for coating industry application. The cured materials are shown in Fig. 9, where extensive bubble formation is clearly visible in the CNF-containing samples. These voids, both large and small, rendered the composites highly heterogeneous and act as stress concentrators

during mechanical loading. As a result, the tensile and impact properties obtained from these samples cannot be considered representative of their intrinsic performance. Nevertheless, limited testing was performed to provide an indicative assessment of mechanical trends.

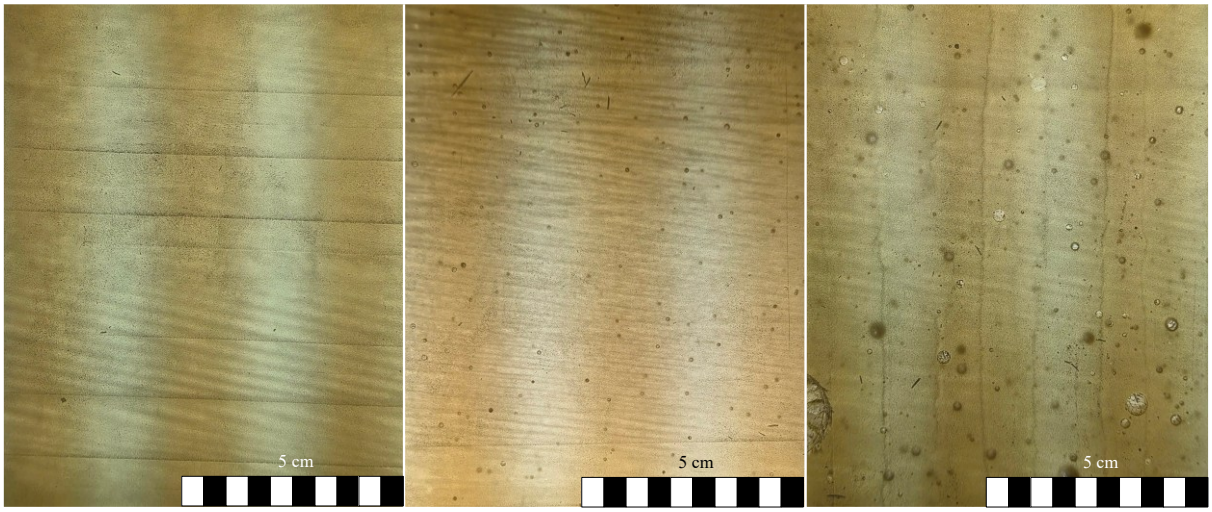


Fig. 9. Cured CNF-PU composites. Left : 0.0% CNF. Middle: 0.67% CNF. Right: 1.33% CNF. Linear patterns on surface stems from CNC router machine. Dots are trapped air.

Two primary mechanisms may contribute to the formation of bubbles within the material: (i) Chemical foaming due to reaction between water and diisocyanate, generating CO_2 gas, or (ii) physical entrapment of air during mixing, followed by insufficient bubble escape due to elevated viscosity. Although nanocellulose is often assumed to introduce moisture because of its hydrophilic nature, the polyol itself is hygroscopic and readily absorbs water from the atmosphere. This is demonstrated in Fig. 10, where the neat polyol – used as received from the supplier – also produced a cured PU matrix containing several large bubbles. In industrial practice, polyols are routinely dried (*e.g.*, at 105 °C) before use to avoid moisture-driven foaming. When performing this same heat treatment on the neat polyol sample, it visually changed from being cloudy to becoming clear – and the resulting cured PU shown in Fig. 9 is bubble free.

In the present study, the CNF masterbatch was previously measured to contain < 0.01% moisture, and the CNF/polyol mixtures were afterwards processed under vacuum at 35 °C for 12 hours, significantly limiting the likelihood of CNF-associated water being the root cause of bubbles. Instead, the most plausible explanation is that CNF addition increased the viscosity of the reactive mixture sufficiently that air introduced during the mixing and curing-agent addition steps could not escape before curing. Such entrapment is a well-known challenge in high-viscosity thermoset formulations containing rheology modifiers and follows Stokes law on terminal velocity of spheres in a fluid – that sphere (*i.e.* bubble) velocity is inversely proportional to viscosity of the fluid. From Fig. 2, the apparent viscosity at the lowest shear rate increased from approximately 0.5 Pa·s in the neat polyol to 56.0 and 346.5 Pa·s for 1.0% and 2.0% CNF samples, meaning that the bubble mobilities in these samples were markedly reduced. This is apparent in Fig. 10; the neat PU reference was free of bubbles; the 0.67% CNF sample contained small bubbles; and the 1.33% CNF sample had both large and small bubbles in its matrix. In practical

applications, this issue is commonly addressed through the use of defoaming additives or by implementing specialised mixing and degassing protocols (Pelton and Flaherty 2003).

A factor that also could play into the mechanical results is the potential degree of alignment of CNFs during curing, as fibre orientation is known as an important factor in composite engineering. Based on the observed rheological behaviour, the CNFs form a dynamic, physically entangled network that is disrupted under shear and rapidly reforms at rest. As curing occurs under essentially quiescent conditions, any alignment induced during mixing is expected to relax prior to matrix solidification. The final material is therefore expected to exhibit a largely isotropic CNF network.



Fig. 10. Neat PU affected by moisture-induced foaming. Cured prior to heat treatment which would have evaporated the residual water. The sample is 410x410 mm.

Mechanical Properties of Cured Samples – Affected by CNFs and Voids

As stated previously, polyol samples were cured with diisocyanate and produced composites with 0%, 0.67%, and 1.33% CNF. All CNF-containing composites exhibited varying degrees of void formation, potentially arising from increased viscosity and limited bubble mobility during curing. These voids introduce substantial heterogeneity, especially in the tensile specimens, and must be considered when interpreting the mechanical results.

The measured tensile properties for the three formulations are summarized in Figs. 11a-c, and the corresponding impact strength are shown in Fig. 11d. To quantitatively assess whether differences between CNF levels were statistically meaningful, one-way ANOVA and pairwise Welch t-tests were performed on the measured means, standard deviations, and sample sizes (three tensile specimens per formulation; two or three for impact tests, depending on CNF level).

The *elastic modulus* (Fig. 11a) increased systematically with CNF loading, from 72.03 MPa (0% CNF) to 93.78 MPa (0.67% CNF) and 164.30 MPa (1.33% CNF). One-way ANOVA confirmed that CNF content had a significant overall effect on modulus ($F = 11.93$, $df = 2,6$; $p < 0.01$). Pairwise Welch t-tests showed trends toward significance for 0% *vs.* 0.67% ($p = 0.059$) and 0% *vs.* 1.33% ($p = 0.053$), although both fell marginally above the $\alpha = 0.05$ threshold due to the limited sample size and high variance of the 1.33% CNF group. Despite this, the statistical analyses and the magnitudes of the means clearly indicate that CNF acts as an effective stiffening agent, consistent with the formation of a percolated fibrillar network within the matrix.

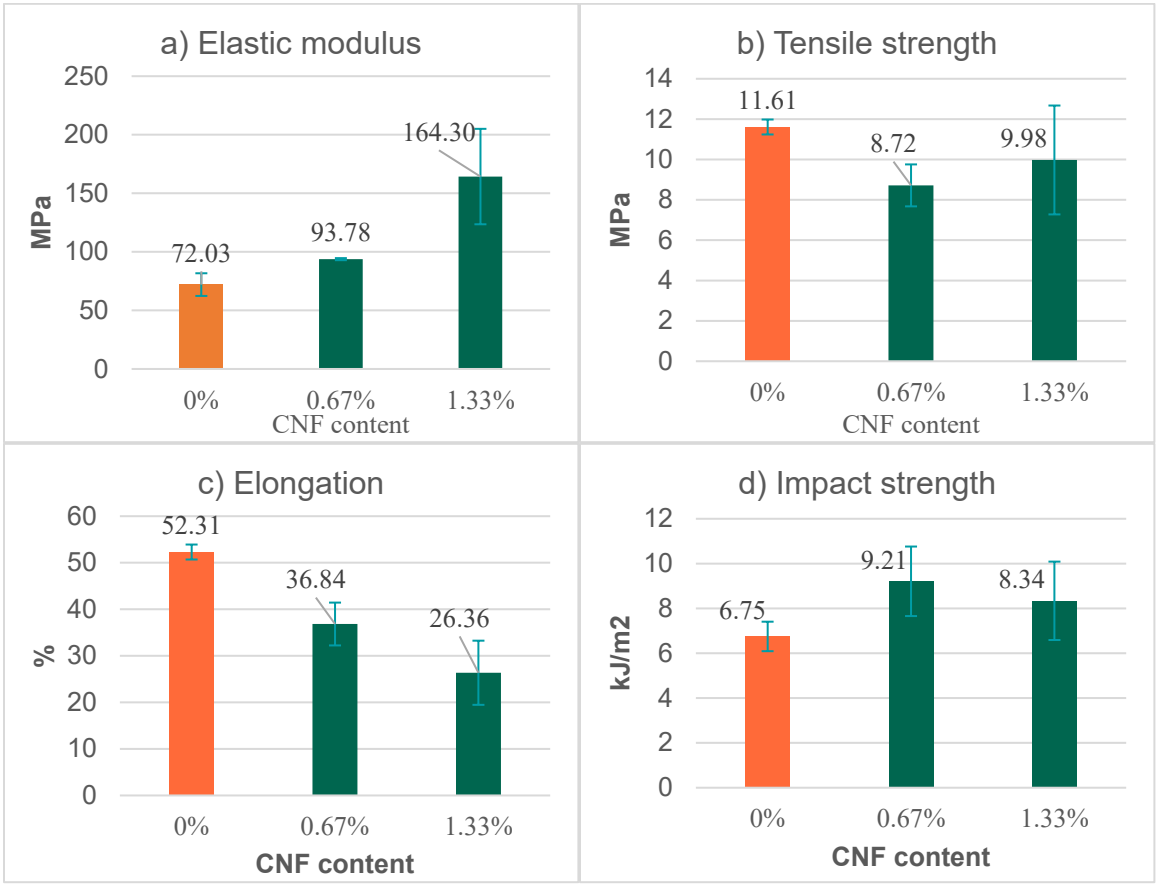


Fig. 11. Mechanical properties from impact and tensile tests. Error bars show standard deviation.

Mean tensile strengths (Fig. 11b) were 11.61 MPa (0%), 8.72 MPa (0.67%), and 9.98 MPa (1.33% CNF). ANOVA yielded no significant overall difference between groups ($F = 2.22$, $df = 2,6$; $p > 0.15$). The only significant pairwise difference occurred between 0% and 0.67% CNF ($p = 0.029$), where the reduction in strength correlates with visible voids rather than any intrinsic weakening by CNF. These findings support qualitative observations: although the CNF network itself is not detrimental, voids act as premature failure sites and dominate the tensile failure behaviour. As can be seen in Fig. 10, the matrix voids were of an even, relatively small size in the 0.67% CNF composite, but the size distribution of voids was much larger for the 1.33% CNF material. The larger spread in void sizes likely correlates to the much wider standard deviation of the latter sample specimens.

Elongation values (Fig. 11c) decreased from 52.3% (0% CNF) to 36.8% (0.67% CNF) and 26.4% (1.33% CNF). ANOVA revealed a highly significant effect of CNF content ($F = 21.54$, $df = 2,6$; $p < 0.01$). Pairwise tests showed that both CNF-containing formulations exhibited significantly lower elongation relative to the reference:

- 0% vs 0.67% CNF: $p = 0.019$
- 0% vs 1.33% CNF: $p = 0.018$

The 0.67% vs 1.33% comparison showed a non-significant trend ($p = 0.104$). These results are fully consistent with the rheological evidence for a progressively stronger fibrillar network. The CNF network increases stiffness but proportionally limits the material's capacity for large-strain deformation.

Impact strength values (Fig. 11d) were 6.75, 9.21, and 8.34 kJ/m² for 0%, 0.67%, and 1.33% CNF. ANOVA detected no statistically significant differences in either impact strength ($F = 1.61$, $df = 2,5$; $p > 0.25$). Pairwise comparisons similarly yielded no significant contrasts (all $p > 0.09$), although the 0.67% CNF samples consistently showed the highest impact values. Figure 12, a SEM image of fractured surface, revealed torn fibres and fibrils embedded within the matrix, indicating mechanical interaction between CNFs and the PU network. The lack of statistical significance therefore reflects high specimen-to-specimen variability, driven primarily by void content, rather than a weak reinforcing effect. Note that the larger fibre observed in Fig. 12 is attributed to residual, not fully fibrillated material remaining after mechanical processing. It does not represent the dominant population, which consists of finer fibrillar structures.

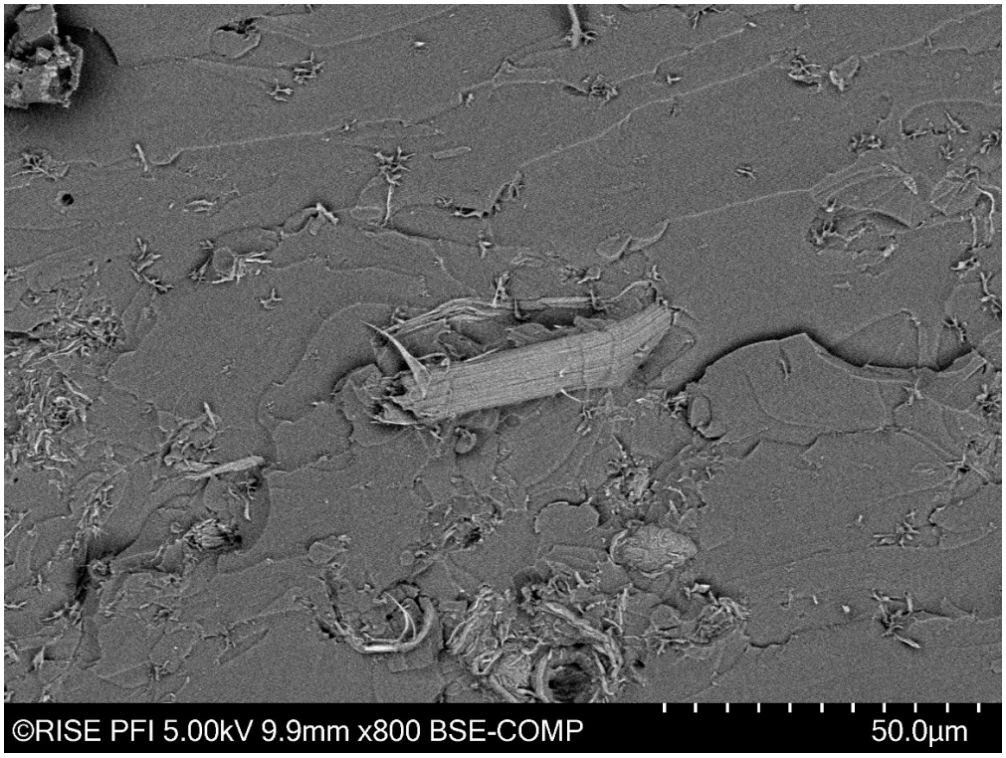


Fig. 12. Fracture site from tensile test of 1.33% CNF sample, showing a torn fibre and smaller fibrils embedded in the matrix

Overall, the mechanical results shown in Figs. 11a-d demonstrate that CNF addition influenced stiffness, toughness, strength, and ductility in distinct ways, with CNF loading and void formation affecting different regions of the stress-strain response. Formation of a rigid, percolated CNF network increase small-strain stiffness but simultaneously restrict the composite's ability to undergo large-strain deformation (Lee *et al*., 2014). Because the elastic modulus is determined in the initial linear region – where deformations remain small and stress concentrations around voids may have not yet been activated – the observed stiffness enhancement primarily reflects the reinforcing effect of the fibrils rather than the presence of bubbles (Ward and Sweeney, 1971). In contrast, tensile strength (Fig. 11b) and impact energy (Fig. 11d) are governed by large-strain or dynamic failure mechanisms and therefore exhibit greater sensitivity to voids and microstructural heterogeneity.

These mechanical results should be considered as indicative rather than definitive due to the presence of voids. Nevertheless, the trends suggest that CNF addition does not inherently degrade composite performance, rather that they become stiffer. The observed reduction in tensile strength appears more strongly correlated with bubble formation than with the presence of CNFs. A void-free composite would likely benefit more fully from the reinforcing potential of the CNF network and may exhibit simultaneous improvements in stiffness and strength. In principle, agglomeration effects of the CNFs could be evaluated through comparison with theoretical reinforcement models (*e.g.*, Halpin-Tsai), but this approach was not viable in the present study due to the bubble formation and the following consequences on mechanical results.

CONCLUSIONS

1. This work demonstrated that cellulose nanofibrils (CNF) can be incorporated into polyurethane systems through a solvent-free polyol-based masterbatch, producing highly fibrillated suspensions with controllable rheological behaviour and measurable mechanical reinforcement. The term polyol here refers to a commercially available hydroxylated soybean oil product.
2. Rheological measurements showed that CNF addition induced strong shear-thinning behaviour, increased low-shear viscosity, and significantly reduced temperature sensitivity relative to the neat polyol. Unlike conventional rheology modifiers, whose performance deteriorates under heat, the CNF network is stabilized primarily through steric interactions and entanglement, enabling it to maintain structural integrity in a temperature range relevant to what occurs during the exothermic curing reaction of a polyurethane coating.
3. Arrhenius-type modelling quantified this effect, showing that increasing CNF loading consistently lowered the activation energy for viscous flow and mitigates viscosity loss at elevated temperatures.
4. Oscillatory measurements revealed that CNF-containing formulations maintained a well-defined linear viscoelastic region, with network-dominated gel-like behaviour emerging at ≥ 2% CNF. The fibril network strengthened the material elastically without extending its strain tolerance, suggesting that CNFs control the magnitude of modulus but not the onset of structural breakdown. Frequency sweeps further confirmed progressive network formation with CNF loading, transitioning from viscoelastic fluid-like behaviour to gel-like response.
5. Mechanical testing of cured composites showed that CNF addition intrinsically increased stiffness and contributed to energy absorption during dynamic loading, as supported by SEM images showing torn fibrils engaged within the fracture surface. However, void formation – arising primarily from air entrapped during mixing and hindered diffusion in high-viscosity CNF/polyol mixtures – dominated tensile strength outcomes and limited interpretation of the intrinsic reinforcing effect.

ACKNOWLEDGMENTS

This work was supported by the Research Council of Norway (grant number 328808). The Research Council of Norway is also acknowledged for the support to the Norwegian Cellulose Laboratory, NORCELlab, project number 322440.

The authors thank Ingebjørg Leirset, Berit Leinsvang, Kenneth Aasarød, Merete Wiig and Steinar Seehuus (RISE PFI), Magnus Sjögren, Alexander Tsigras, Petter Syverstad, Bjørn Einar Sundal (Norske Skog Saugbrugs) for skilful experimental work. Norske Skog Saugbrugs is kindly thanked for providing samples used throughout this work.

Conflict of Interest

Authors Kristin Syverud, Gary Chinga Carrasco, Jost Ruwoldt declare they have no competing interests. Authors Simen Prang Følkner and Dag Molteberg are employed at Norske Skog Saugbrugs, which provided CNF MB samples and funds the industry doctorate in which this work has been conducted.

Use of Generative AI

During the preparation of this work the authors used ChatGPT 4o and MS365 Copilot in order to improve text readability. After using this tool/service, the authors reviewed and edited the content as needed and takes full responsibility for the content of the published article.

REFERENCES CITED

Barnes, H. A., Hutton, J. F., and Walters, K. (1989). *An Introduction to Rheology*, Elsevier.

Bello, K. O., and Yan, N. (2024). "Mechanical and insulation performance of rigid polyurethane foam reinforced with lignin-containing nanocellulose fibrils," *Polymers* 16(15), article 2119. https://doi.org/10.3390/polym16152119

Bird, R. B., Stewart, W. E., and Lightfoot, E. N. (2006). *Transport Phenomena*, John Wiley & Sons.

Chemicals strategy - Environment - European Commission. (2025). https://Environment.Ec.Europa.Eu/Strategy/Chemicals-Strategy_en (Accessed 2025-12-07).

Chen, Y., Yu, Z., Oguzlu, H., Jiang, J., Cho, M. J., Karaaslan, M., Renneckar, S., and Jiang, F. (2021). "Superelastic and flexible 3D printed waterborne polyurethane/ cellulose nanofibrils structures," *Additive Manufacturing* 46, article 102107. https://doi.org/10.1016/j.addma.2021.102107

Commission Regulation (EU) 2020/1149 of 3 August 2020 Amending Annex XVII to Regulation (EC) No 1907/2006 of the European Parliament and of the Council Concerning the Registration, Evaluation, Authorisation and Restriction of Chemicals (REACH) as Regards Diisocyanates (Text with EEA Relevance), Pub. L. No. Vol. 252 (2020).

Directive 2004/42/EC of the European Parliament and of the Council of 21 April 2004 on the Limitation of Emissions of Volatile Organic Compounds Due to the Use of

Organic Solvents in Certain Paints and Varnishes and Vehicle Refinishing Products and Amending Directive 1999/13/EC (2021).

Domínguez, J. C. (2018). "Rheology and curing process of thermosets," in: *Thermosets*, Second Edition, Elsevier, pp. 115-146.

European Commission. "COMMISSION REGULATION (EU) 2023/2055 of 25 September 2023 Amending Annex XVII to Regulation (EC) No 1907/2006 of the European Parliament and of the Council Concerning the Registration (Text with EEA Relevance), Pub. L. No. Vol. 238 (2023).

Følkner, S. P., Molteberg, D., Axelsson, P., Carrasco, G. C., and Syverud, K. (2025). "Tracking fibre to fibrillation development for industrial production of nanocellulose," *Cellulose* 32, 9367-9383. https://doi.org/10.1007/s10570-025-06774-7

Følkner, S. P., Molteberg, D., Carrasco, G. C., and Syverud, K. (2026). "Rheological, mechanical, and hygroscopic performance of CNF masterbatches in epoxy systems," *Industrial Crops & Products* 247, article 123533. https://doi.org/10.1016/j.indcrop.2026.123533

Haseebuddin, S., Raju, K. V. S. N., Krishna, D., Reddy, P. J., and Yaseen, M. (1996). "Temperature dependence of viscosity of polyurethane polyol solutions: Application of rheological models," *Journal of Applied Polymer Science* 59(1), 29-36. https://doi.org/10.1002/(SICI)1097-4628(19960103)59:1<29::AID-APP5>3.0.CO;2-O

Hepburn, C. (1992). *Polyurethane Elastomers*, Springer.

Hinrichsen, G. (1993). *Polyurethane Handbook*, 2nd Ed., G. Oertel (ed.), *Hanser Publishers.*

Hubbe, M. A., Tayeb, P., Joyce, M., Tyagi, P., Kehoe, M., Dimic-Misic, K., and Pal, L. (2017). "Rheology of nanocellulose-rich aqueous suspensions: A review," in: *BioResources* 12(4), 9556-9661. https://doi.org/10.15376/biores.12.4.Hubbe

Iotti, M., Gregersen, Ø. W., Moe, S., and Lenes, M. (2011). "Rheological studies of microfibrillar cellulose water dispersions," *Journal of Polymers and the Environment* 19(1), 137-145. https://doi.org/10.1007/s10924-010-0248-2

Lee, K. Y., Aitomäki, Y., Berglund, L. A., Oksman, K., and Bismarck, A. (2014). "On the use of nanocellulose as reinforcement in polymer matrix composites," *Composites Science and Technology* 105, 15-27. https://doi.org/10.1016/j.compscitech.2014.08.032

Leng, W., Li, J., and Cai, Z. (2017). "Synthesis and characterization of cellulose nanofibril-reinforced polyurethane foam," *Polymers* 9(11), article 597. https://doi.org/10.3390/polym9110597

Magnin, A., Pollet, E., Phalip, V., and Avérous, L. (2020). "Evaluation of biological degradation of polyurethanes," in: *Biotechnology Advances*, Vol. 39, Elsevier Inc. https://doi.org/10.1016/j.biotechadv.2019.107457

Montarnal, D., Capelot, M., Tournilhac, F., and Leibler, L. (2011). "Silica-like malleable materials from permanent organic networks," *Science* 334(6058), 962-965. https://doi.org/10.1126/science.1211649

Noble, K.-L. (1997). "Waterborne polyurethanes," *Progress in Organic Coatings* 32, 131-136. https://doi.org/10.1016/S0300-9440(97)00071-4

Pei, A., Malho, J. M., Ruokolainen, J., Zhou, Q., and Berglund, L. A. (2011). "Strong nanocomposite reinforcement effects in polyurethane elastomer with low volume

fraction of cellulose nanocrystals," *Macromolecules* 44(11), 4422-4427. https://doi.org/10.1021/ma200318k

Pelton, R., and Flaherty, T. (2003). "Defoamers: Linking fundamentals to formulations," *Polymer International 52*, 479-485. https://doi.org/10.1002/pi.1203

Randall, D., and Lee, S. (2002). *The Polyurethanes Book*, Wiley.

Rouyer, F., Cohen-Addad, S., and Höhler, R. (2005). "Is the yield stress of aqueous foam a well-defined quantity?" *Colloids and Surfaces A: Physicochemical and Engineering Aspects*, *263*(1-3 SPEC. ISS.), 111-116. https://doi.org/10.1016/j.colsurfa.2005.01.025

Saunders, K. J. (1988). "Polyurethanes," in: *Organic Polymer Chemistry: An Introduction to the Organic Chemistry of Adhesives, Fibres, Paints, Plastics and Rubbers*, Springer Netherlands, pp. 358-387.

Septevani, A. A., Evans, D. A. C., Annamalai, P. K., and Martin, D. J. (2017). "The use of cellulose nanocrystals to enhance the thermal insulation properties and sustainability of rigid polyurethane foam" *Industrial Crops and Products* 107, 114-121. https://doi.org/10.1016/j.indcrop.2017.05.039

Shafiei-Sabet, S., Hamad, W. Y., and Hatzikiriakos, S. G. (2012). "Rheology of nanocrystalline cellulose aqueous suspensions," *Langmuir* 28(49), 17124-17133. https://doi.org/10.1021/la303380v

Simon, S., Subramanian, S., Gao, B., and Sjöblom, J. (2015). "Interfacial shear rheology of gels formed at the oil/water interface by tetrameric acid and calcium ion: Influence of tetrameric acid structure and oil composition," *Industrial and Engineering Chemistry Research* 54(35), 8713-8722. https://doi.org/10.1021/acs.iecr.5b02165

Sinquefield, S., Ciesielski, P. N., Li, K., Gardner, D. J., and Ozcan, S. (2020). "Nanocellulose dewatering and drying: Current state and future perspectives," *ACS Sustainable Chemistry and Engineering* 8(26), 9601-9615. https://doi.org/10.1021/acssuschemeng.0c01797

Ward, I. M., and Sweeney, J. (1971). *Mechanical Properties of Solid Polymers Mechanical Properties of Solid Polymers*, Wiley-Interscience.

Wicklein, B., Kocjan, A., Salazar-Alvarez, G., Carosio, F., Camino, G., Antonietti, M., & Bergström, L. (2015). "Thermally insulating and fire-retardant lightweight anisotropic foams based on nanocellulose and graphene oxide," *Nature Nanotechnology* 10(3), 277-283. https://doi.org/10.1038/nnano.2014.248

Williams, M. L., Landel, R. F., and Ferry, J. D. (1955). "Temperature dependence of relaxation mechanisms the temperature dependence of relaxation mechanisms in amorphous polymers and other glass-forming liquids," *Journal of the American Chemical Society* 77, 3701-3707. https://doi.org/10.1021/ja01619a008

Winter, H. H., and Chambon, F. (1986). "Analysis of linear viscoelasticity of a crosslinking polymer at the gel point," *Journal of Rheology* 30(2), 367-382. https://doi.org/10.1122/1.549853

Yang, W., Zhu, Y., Liu, T., Puglia, D., Kenny, J. M., Xu, P., Zhang, R., and Ma, P. (2023). "Multiple structure reconstruction by dual dynamic crosslinking strategy inducing self-reinforcing and toughening the polyurethane/nanocellulose elastomers," *Advanced Functional Materials* 33(12), article 202213294. https://doi.org/10.1002/adfm.202213294

Zhou, X., Sethi, J., Geng, S., Berglund, L., Frisk, N., Aitomäki, Y., Sain, M. M., and Oksman, K. (2016). "Dispersion and reinforcing effect of carrot nanofibers on biopolyurethane foams," *Materials and Design* 110, 526-531. https://doi.org/10.1016/j.matdes.2016.08.033

Article submitted: 17th of April 2026; Peer review completed: May 9, 2026; Revised version received: June 1, 2026; Accepted: June 29, 2026; Published: July 9, 2026.
DOI: 10.15376/biores.21.3.7949-7973